

Article

Tribocorrosion Behaviour of SUS430 Stainless Steel in Aqueous Solutions with Different pH

Rongguang Wang ^{1,*} , Yuto Ohgata ², Yunhui Li ², Tian Xiao ² and Masaharu Honda ³

¹ Department of Mechanical Systems Engineering, Hiroshima Institute of Technology, Hiroshima 731-5193, Japan

² Graduate School of Science and Technology, Hiroshima Institute of Technology, Hiroshima 731-5193, Japan

³ Taiyo Electric Ind. Co., Ltd., Yamate, Fukuyama 720-0092, Japan; nsl3171n@gmail.com

* Correspondence: wangrg@cc.it-hiroshima.ac.jp

Abstract: To reveal the influence of passive film on the tribocorrosion behaviour of stainless steel, SUS430 was loaded at 2.0 N or 10.0 N in aqueous solutions with various pH from 1.0 to 10.0. The pure wear behaviour was investigated in the air for comparison. The polarization behaviour, the morphology of the worn or tribocorroded surface, and the depth profiles of the formed groove were measured to discuss the mechanism. The passive state was confirmed at pH = 7.0 and 10.0, but vanished at pH = 1.0 and 2.0. The pure wear in air depended on the applied loads, rather than the sliding time. On the other hand, the tribocorrosion in deionised water was much smaller than the pure wear in air. Under a load of 2.0 N, the tribocorrosion at pH = 1.0 was weaker than pH = 2.0. However, the situation reversed when increasing the load to 10.0 N. The tribocorrosion in neutral and alkaline solutions is considerably smaller than in acid solutions.

Keywords: stainless steel; passive film; tribocorrosion; corrosion; wear; pH; load



Citation: Wang, R.; Ohgata, Y.; Li, Y.; Xiao, T.; Honda, M. Tribocorrosion Behaviour of SUS430 Stainless Steel in Aqueous Solutions with Different pH. *Coatings* **2023**, *13*, 1539. <https://doi.org/10.3390/coatings13091539>

Academic Editor: Claudio Mele

Received: 13 August 2023

Revised: 26 August 2023

Accepted: 28 August 2023

Published: 1 September 2023



Copyright: © 2023 by the authors. Licensee MDPI, Basel, Switzerland. This article is an open access article distributed under the terms and conditions of the Creative Commons Attribution (CC BY) license (<https://creativecommons.org/licenses/by/4.0/>).

1. Introduction

Sliding produces physical work in machinery, but simultaneously brings about the wear of materials. Wear can be classified as adhesive, abrasive, fretting, and fatigue based on different mechanisms, depending on the composition/microstructure of the materials, the applied load, and the working environment. In an aqueous solution, the corrosion of metal causes the so-called tribocorrosion. Tribocorrosion is generally greater than the separated dry wear or the chemical dissolution, usually accelerating the deterioration of equipment [1].

Stainless steel is widely used due to its high strength, ductility, and corrosion resistance. Its tribocorrosion behaviour has been well investigated [2–6]. The key point is the steel's passive film, which determines the corrosion resistance, mechanical properties, and tribocorrosion behaviour in various environments. In particular, the pH of a solution largely affects the thickness and composition of the passive film. The film becomes thin or disappears in an acid solution, while the thick film forms in a neutral or alkaline solution [7]. The composition generally changes from oxides to hydroxides with increasing pH [8–10]. All the above differences in passive film largely affect the tribocorrosion of stainless steel. In an acid environment, stainless steel suffers from fast dissolution with hydrogen involvement, while in neutral or alkaline solution, the passive film is composed of oxide and hydroxide [7,11–13]. This means different surficial materials for tribocorrosion. The passive film can be worn and detached depending on the load level, followed by repair after sliding [2,14]. These factors cause the complicated mechanism of tribocorrosion [2]: the accelerated corrosion due to the removal of the passive film by wear and the accelerated wear due to the yield of the unstable surface by corrosion.

Many studies on the tribocorrosion behaviour of stainless steel focused on the passive film's destruction and repair in weak acid or neutral/alkaline solution. The formation

and removal of the passive film can be controlled by adjusting the pH. A passive film was recently confirmed in a solution with pH = 1.5 during tribocorrosion for a type 430 steel (16Cr) galvanically coupled with a half-moon-shaped graphite: wear accelerated corrosion occurred under that condition [6]. The noble graphite brought the potential of the steel from the active zone to the passive zone. The tribocorrosion behaviour of bare stainless steels without passive film has rarely been studied, perhaps due to its few field applications. However, with daily changes in severe working conditions for machinery, the application of bare stainless steel or other alloys becomes inevitable. Therefore, it is necessary to systemically investigate and discuss the tribocorrosion behaviour of stainless steels or alloys from bare surfaces to passive film-covered surfaces.

Hydrogen bubbles in acid solution and their detachment or reattachment from/to the surface are essential factors in discussing the tribocorrosion behaviour in acid solution. These will affect the sliding zone's mechanical wear and the total surface's corrosion reaction. Therefore, focusing on the changes of the entire surface should help in understanding the mechanism of tribocorrosion. However, the influence of a sliding zone on unworn surroundings has not been well investigated. Furthermore, the co-influence of load and pH on the tribocorrosion of stainless steel or alloy should be clarified to enhance the integrity of machinery in harsh conditions.

To clarify the above issues, in this study, the ferritic stainless steel SUS430, which is usually applied in structures, automobiles, electrical appliances, and daily commodities, was chosen as the test material due to the easily controlled formation/vanishing behaviour of passive film based on the pH of the solution. Note that its general resistance to tribocorrosion is comparable to other common stainless steels. The galvanic effect between the worn and the unworn zones was considered without applying any constant potential to the steel [15,16] or coupling with other materials [6]. Tribocorrosion was carried out in aqueous solutions with a variety of pH values under different applied loads and sliding periods and compared to pure wear behaviour in the air. After the tests, the formed groove and its surroundings were observed with a laser microscope and the groove's cross-sectional area and volume accordingly obtained. Finally, the tribocorrosion behaviour was compared and the corrosion depth, the deformation region, the pH value, the sliding time, the coefficient of friction, and the Archard wear coefficient were discussed.

2. Experimental

A commercially supplied ferritic stainless steel SUS430 plate (JIS G 4304-2015) with the following chemical composition was used as the test material: 0.04 mass% C; 0.24% Si; 0.62% Mn; 0.031% P; 0.007% S; 16.47% Cr; 0.35% Ni; and the balanced Fe. Its ultimate tensile strength (σ_u), yield strength (σ_y) and elastic modulus (E_1) are 486 MPa, 324 MPa and 200 GPa, respectively. The plate was machined to 15 mm \times 15 mm \times 5 mm and polished with number 2000 emery paper before it was used as a specimen. As shown in Figure 1 (a: left drawing), some specimens were sealed with silicone sealant, exposing only a 10 mm \times 10 mm polished area for the polarization measurement. The other specimens were embedded into a phenol-formaldehyde resin for the wear or tribocorrosion test (Figure 1a: right drawing)). As shown in Table 1, the solutions for polarization and tribocorrosion were laboratory-prepared with deionised water, H₂SO₄, and NaOH using a pH meter (Horiba: LAQUA D-72). The pH values were chosen by considering their relationship with the stability of passive film [7]. Considering the uniform ion strength [17] or the conductivity of the solution, 0.05 M Na₂SO₄ was added to the solutions of pH = 7.0 and 10.0.

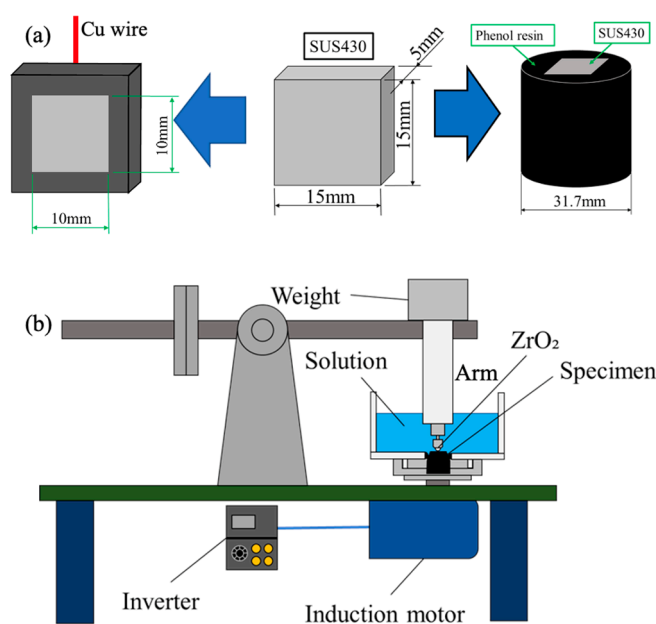


Figure 1. Assembly of the specimen (a) and the tribocorrosion tester (b).

Table 1. Solutions used in polarization and tribocorrosion.

pH	Solution	Ion Strength
1.0	0.05 M H ₂ SO ₄	0.150
2.0	0.005 M H ₂ SO ₄	0.015
2.7	0.001 M H ₂ SO ₄	0.003
7.0	0.05 M Na ₂ SO ₄	0.150
10.0	0.0001 M NaOH + 0.05 M Na ₂ SO ₄	0.150

In solutions with pH = 7.0 and 10.0, a preliminary polarization was applied at a constant potential of -1.0 V for 60 s to stabilise the surface. The polarization was carried out by a potentiostat (Solartron Analytical: 1285A) in a glass cell with a counter electrode of the platinum plate and a reference one of saturated calomel electrode (SCE). After naturally keeping the specimen in the designated solution for 300 s, the potential was swept from -0.7 V to 1.0 V (vs. SCE) to obtain a full polarization curve from the cathodic to the anodic reactions in all the solutions. The polarization curve obtained the corrosion potential, and the Mansfeld fitting method [7,18] was applied to obtain the corrosion current density.

Figure 1b shows that a home-made acrylic cell was mounted to a frictional resistance tester (Heidon Type: 20) for wear and tribocorrosion tests. At least two tests were carried out to confirm the reproducibility. A ZrO₂ ball (elastic modulus (E_2): 210 GPa) with a diameter of 5.0 mm was fixed to the insulated head of the arm for applying load. Except in air, 150 mL solution was poured into the cell, and an induction motor rotated the specimen at 60 rpm for 1.0 and 3.0 h under a load (F) of 2.0 N or 10.0 N. The ball's rotation radius (R) was set to 5.0 mm through a vernier scale; therefore, a sliding speed of 31.4 mm/s was performed. The torque (T) of the induction motor was measured to calculate the coefficient of friction (μ) with Equation (1).

$$\mu = \frac{T}{FR} \quad (1)$$

After the test, the specimen was ultrasonically cleaned in water and acetone. Four crossed positions of the formed groove were observed with a laser microscope (Olympus Co.: LEXT OLS4000) to obtain the width, the maximum depth, and the cross-sectional

groove area (hereinafter CSGA: S_1 – S_4). The volume of the entire groove was then calculated from Equation (2) [19].

$$V = \frac{\pi R(S_1 + S_2 + S_3 + S_4)}{2} \quad (2)$$

The CSGA values were obtained from the hatching parts in Figure 2b–d. Except at pH = 1.0, the baseline from the neighbouring surface was used (Figure 2b: A, B). In the case of pH = 1.0, two baselines were set: the neighbouring corroded surface (Figure 2c; A, B) and the original faraway surface without corrosion (Figure 2d; C). The original faraway surface was reserved by shielding the four corners with Teflon tape (Figure 2a). Different baselines resulted in different values of CSGA.

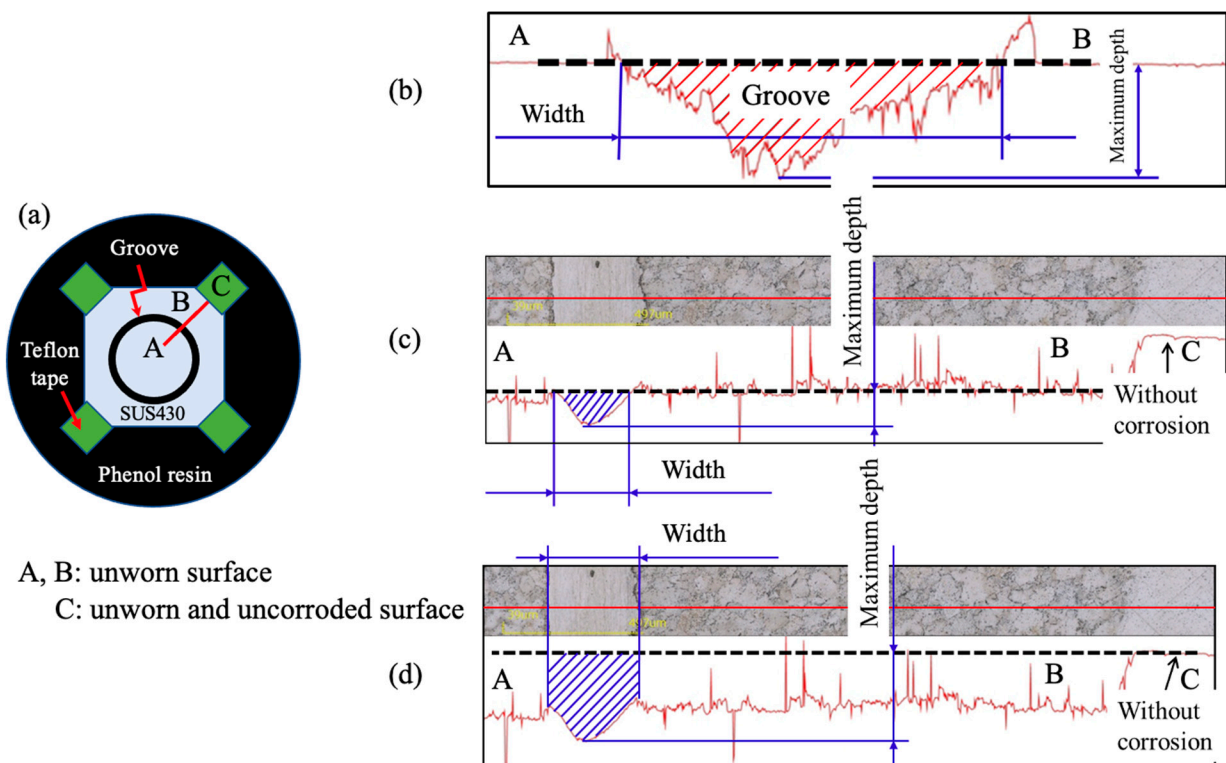


Figure 2. Specimen after wear or tribocorrosion (a) and determination of groove width, maximum depth, and cross-sectional area (b–d).

Note that hereinafter the “free surface” means the surface of a specimen for immersion or polarization, which is free from sliding (see Figure 1a: left). The specimen was not connected to the frictional resistance tester in this case. On the other hand, the “unworn surface” means the partial surface of a specimen for tribocorrosion, except for another surface suffering from the sliding of the ZrO_2 ball (see Figure 2a: A, B).

3. Results and Discussion

3.1. Corrosion Behaviour

Figures 3 and 4 show the polarization curves, the corrosion potential (E_{corr}), and the corrosion current density (i_{corr}) of SUS430 steel in aqueous solutions with a variety of pH values from 1.0 to 10.0. The solution was exposed to air in an aerated condition in this measurement. In the polarization curves, three potentials corresponding to the zero current appeared at pH = 1.0, 2.0, and 2.7. Here, the left one was treated as the E_{corr} . The other two were caused by the higher oxygen reduction current than the passivation current. The cathodic current zone at the noble (passive) side, which corresponds to the excessive oxygen reduction [20], disappeared in a confirmed polarization in a deaerated solution. The corrosion current density was obtained by a Mansfeld fitting method [18], in which

the polarization data within $E_{\text{corr.}} \pm 5$ mV (at pH = 1.0, 2.0, and 2.7) and $E_{\text{corr.}} \pm 15$ mV (at pH = 7.0, and 10.0) were used. The cathodic slope was directly obtained from the cathodic curve, while the anodic slope was determined by fitting the Mansfeld curve.

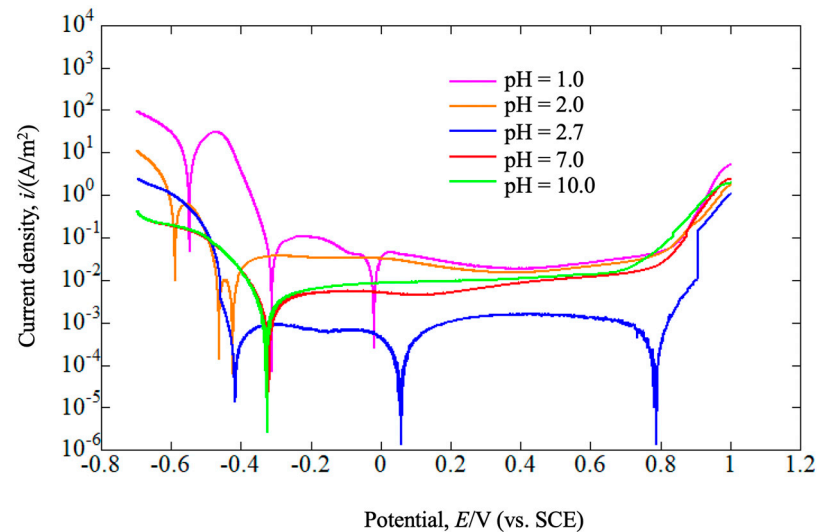


Figure 3. Polarization curves obtained in various solutions with different pH.

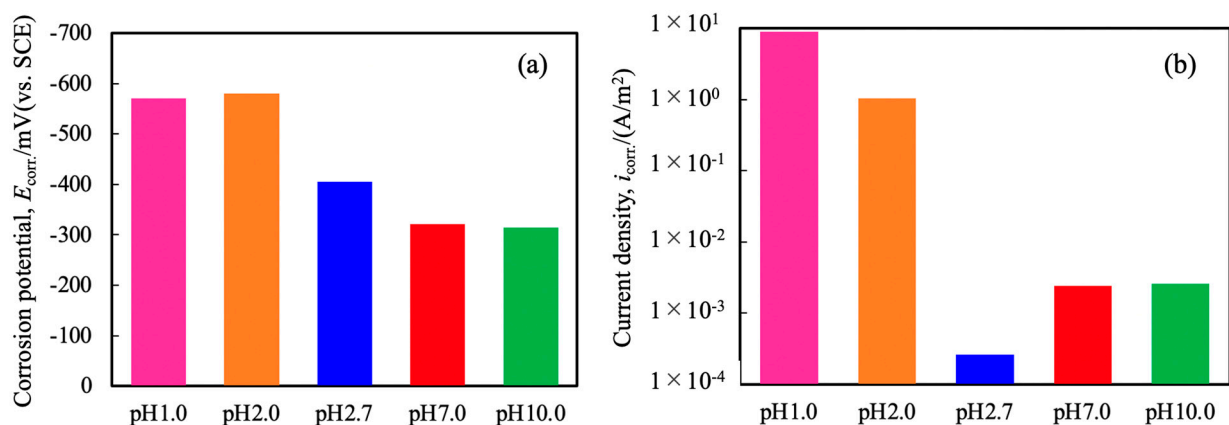


Figure 4. Corrosion potential (a) and corrosion current density (b) obtained in various solutions with different pH.

The polarization curves at pH = 7.0 and 10.0 were almost the same. The corrosion potential became noble with the pH increase from 1.0 to 10.0 (Figure 4a). At pH = 1.0 and 2.0, the corrosion potential dropped below -400 mV. By referring to the in situ-confirmed disappearance of the passive film of SUS304 stainless steel by EC-AFM technology in solutions at pH < 2.7 (with corrosion potential lower than -400 mV) [7] and other reports [21–23], here, both the largely decreased potential (Figure 4a) and the drastically increased corrosion current density (Figure 4b) indicate the loss of passive film from the steel surface. On the other hand, a stable passive film should have covered the surface at pH = 7.0 and 10.0 based on their noble potential and low corrosion current density. The passive film at pH = 2.7 should be in an unstable or transient state [7]. The formation of passive film is related to the hydration of metal atoms followed by dehydration or deprotonation [12].

Except for the lowest value at pH = 2.7, the corrosion current density decreased with pH increase, which corresponds to the above judgment of the presence or the absence of passive film. Except for pH = 2.7, all other passive current densities converged to a narrow range. The low corrosion current density and passive current density at pH = 2.7 were

ascribed to the solution's low conductivity without Na_2SO_4 . The state of the passive film and the corrosion current should primarily affect the tribocorrosion behaviour, which will be investigated later.

The steel immersion was also carried out in a solution at $\text{pH} = 1.0$ with different dissolved oxygen levels. Figure 5 shows the weight loss with immersion time, showing the almost unchanged dissolution rate. In either air exposure or deaeration, the polarization curves (here omitted), except for the difference in the cathodic current (oxygen reduction) at the noble (passive) side, were almost the same.

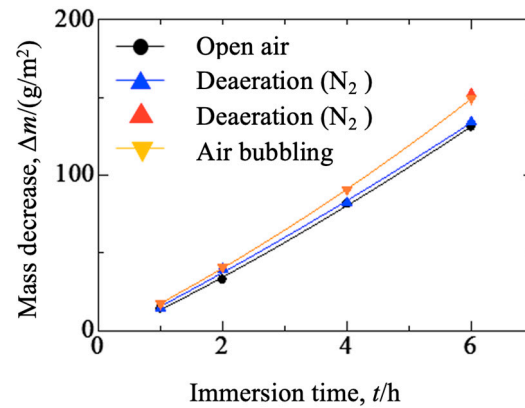


Figure 5. Mass decrease in solution with $\text{pH} = 1.0$ at different concentration levels of dissolved oxygen.

3.2. Wear or Tribocorrosion Behaviour in Air or Water

In the air and under a load of 2.0 N, the obtained CSGAs after 1.0 h and 3.0 h are almost identical (Figure 6a₁). The error bars show the standard deviation. The wear grooves (Figure 6a₂,a₃) show severe wear after cracking and fracturing. Under the static point contact at a load of 2.0 N from a ZrO_2 ball to SUS430 steel, the mean Hertz stress (p_{mean}) on the limited contact area can be calculated as 622 MPa ($= 1.92\sigma_y$) from Equation (3) and Equation (4) [24,25]. Here, r ($= 2.5$ mm) is the radius of the ZrO_2 ball, F is the applied load, and E_1 , E_2 , ν_1 , and ν_2 are the elastic modulus and the Poisson ratios of SUS430 and ZrO_2 , respectively.

$$p_{\text{mean}} = \frac{2}{3\pi} \left(\frac{3FE^2}{2r^2} \right)^{\frac{1}{3}} \quad (3)$$

$$\frac{1}{E} = \frac{1}{2} \left(\frac{1 - \nu_1^2}{E_1} + \frac{1 - \nu_2^2}{E_2} \right) \quad (4)$$

In general, the Hertz stress at $1.1\sigma_y$ causes a region of plastic deformation at the interior of the steel with a depth of 0.47α (α : radius of contact area) [24,25].

$$\alpha = \left(\frac{3Fr}{2E} \right)^{\frac{1}{3}} \quad (5)$$

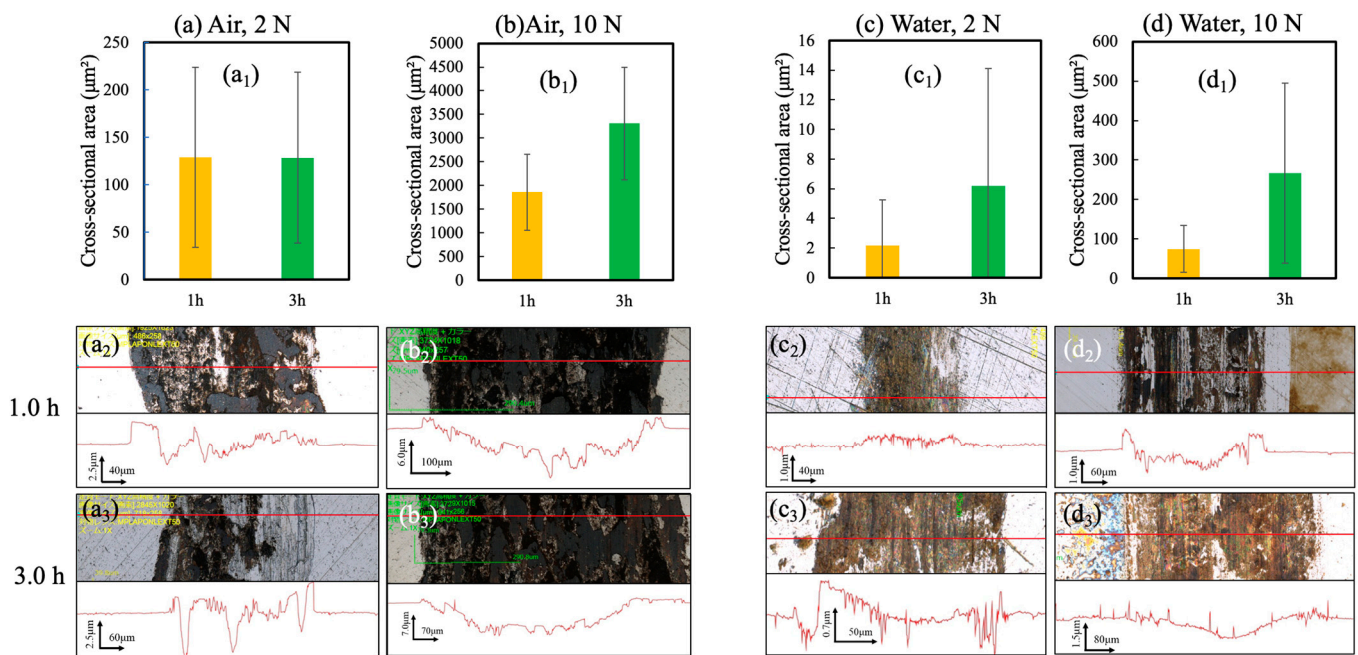


Figure 6. Grooves and the corresponding cross-sectional groove areas after wear in the air (a,b) and after tribocorrosion in deionised water (c,d) under the load of 2 N for 1.0 and 3.0 h.

The higher Hertz stress that is applied, the wider the plastic region appears. Note that even a slight loss of the ball from the contact point will enlarge the contact area, resulting in much smaller lower stress levels than the calculated one. On the other hand, shear stress further occurs along the sliding direction during a dynamic movement. Under a load of 2.0 N, the plastic region is limited and not significantly expanded from the contact point. Therefore, the wear was not as severe as at 10.0 N. The unchanged CSGA after 1.0 and 3.0 h sliding can be mainly ascribed to the accumulation of wear particles on the groove. Even under this low stress and slight wear of the ball, fatigue fracture, related to the elastic shakedown [26], occurs in surficial and sub-surficial metal and produces wear particles. Free and hard particles sliding between the ZrO_2 ball and the steel can play the role of a third body in abrasive wear [2,14]. The cyclically crushed powder would also adhere to the steel, which becomes a hard layer due to the oxidization and the internal residual stress [27].

On the other hand, under the load of 10.0 N, the mean Hertz stress was calculated as 1060 MPa ($= 3.27\sigma_y$). In this case, at least at the early sliding stage, without the occurrence of the wear of the ball, the interior plastic region is greatly enlarged to the surficial deformation under the contact point. Hence, the CSGA under 10.0 N (Figure 6b₁) climbed to more than 10 times that under 2.0 N. The CSGA under 10.0 N also apparently increased when prolonging the sliding time. In the case of considering the wear of the ball, the actual stress level will essentially decrease. Perhaps the accumulation of powder under 10.0 N became less due to the enhanced removal ability of the ZrO_2 ball. In addition, broader wear cycles were observed under 10.0 N.

The CSGAs obtained in deionised water (Figure 6c,d; without Na_2SO_4) were smaller than in the air. This was ascribed to the water's lubrication effect and the passivated surface's existence: a smaller coefficient of friction at 0.43 in water than that at 0.66 in the air. This will be shown later. Under the load of 2.0 N, the groove (Figure 6c₂,c₃) became wider with the increase in sliding time. From the profile after 1.0 h sliding (Figure 6c₂), the groove became even higher than the original surface, which is strong evidence of the accumulation of wear particles. Severe tribocorrosion occurred under a load of 10.0 N than 2.0 N. The wear particle flowed out to the solution, leaving a groove. Considering the

passivation tendency of SUS430 in water is strong, the passive film could also significantly influence the above plastic deformation [28–30].

3.3. Tribocorrosion Behaviour in Solutions with Various pH

Figures 7–10 depict the CSGAs, the morphologies, and the depth profiles of the formed grooves after sliding in solutions with various pH under different loads, respectively. Only at pH = 1.0 does apparent corrosion occur from the unworn surface (without direct contact with the ZrO₂ ball); therefore, two types of CSGA based on the original and the corroded surfaces were drawn (Figures 7 and 8). Their difference corresponds to the corroded depth.

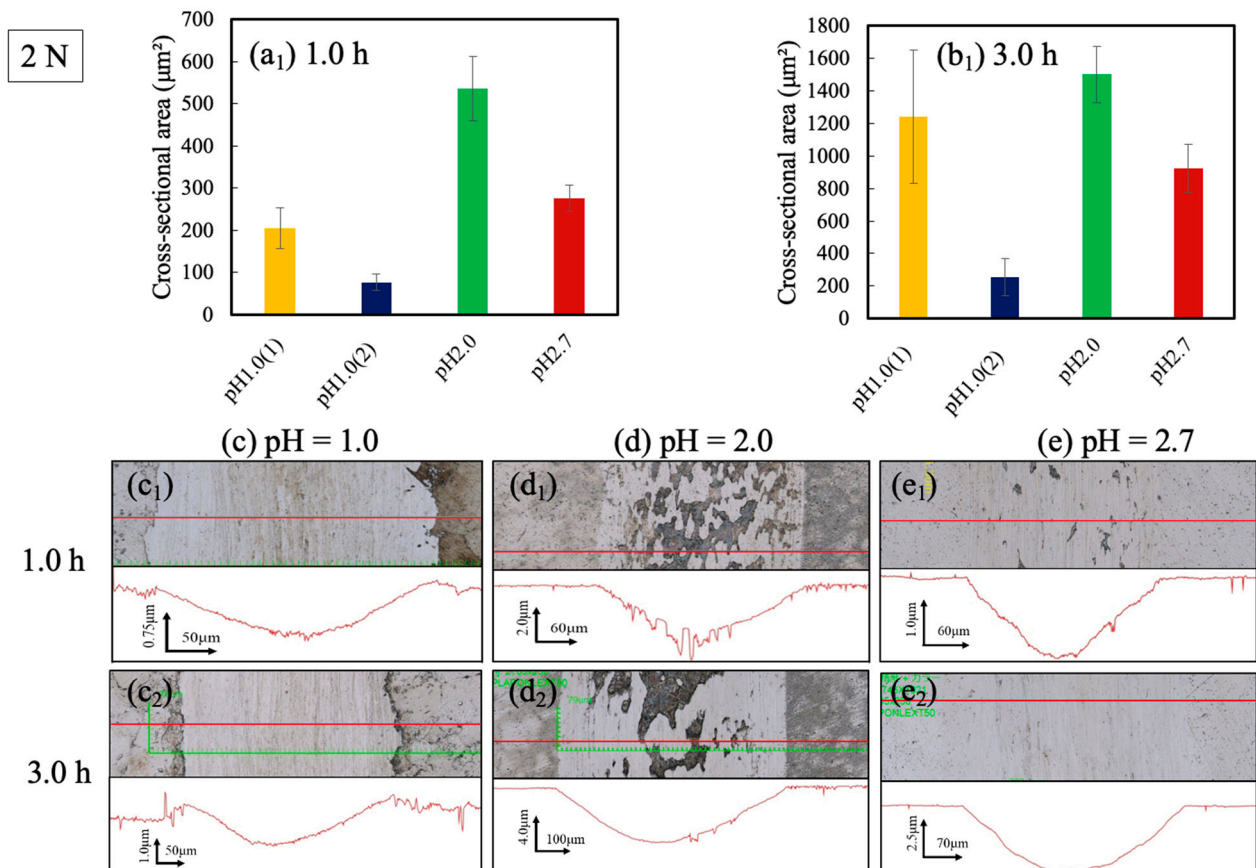


Figure 7. Grooves and the corresponding cross-sectional groove areas after tribocorrosion in solutions with pH = 1.0–2.7 (c–d) under a load of 2 N for 1.0 h (a₁) and 3.0 h (b₁).

3.3.1. Tribocorrosion in Acid Solutions

At pH = 1.0, the ratios of CSGA based on the original surface for 3.0 h vs. 1.0 h sliding are 6.0 (under 2.0 N; Figure 7) and 4.7 (under 10.0 N; Figure 8), respectively. Remarkably, under 2.0 N, the CSGA at pH = 1.0 was even smaller than at pH = 2.0, indicating their different tribocorrosion mechanism. Significantly different from values obtained in air and water (Figure 6), the groove at pH = 1.0 and under 2.0 N was smooth, indicating the simultaneously occurrence of wear and the loss of wear particles. The wear particles might have dissolved or flowed out to the solution. Inoue and Tsuchiya suggested that an increase in the cathodic reaction occurred on the freshly cracked surface of stainless steel in acid solution with low corrosion potential [31,32]. Therefore, the dissolution of wear particles here should be evident for the enhanced cathodic reaction from the worn surface. Under the load of 10.0 N, the groove surface (Figure 8c₁,c₂) became rougher, leaving small pits (black) after 1.0 h and large concaves (bright zones) after 3.0 h.

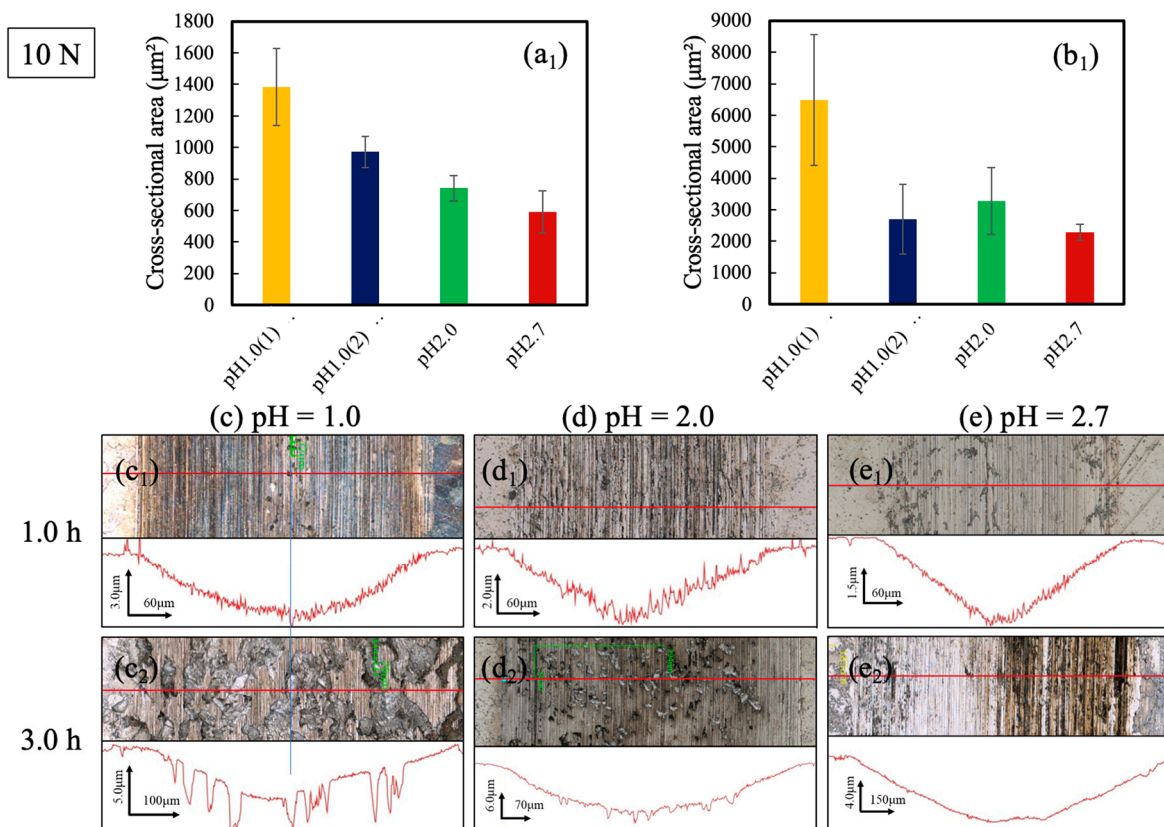


Figure 8. Grooves and the corresponding cross-sectional groove areas after tribocorrosion in solutions with pH = 1.0–2.7 (c–d) under a load of 10 N for 1.0 h (a₁) and 3.0 h (b₁).

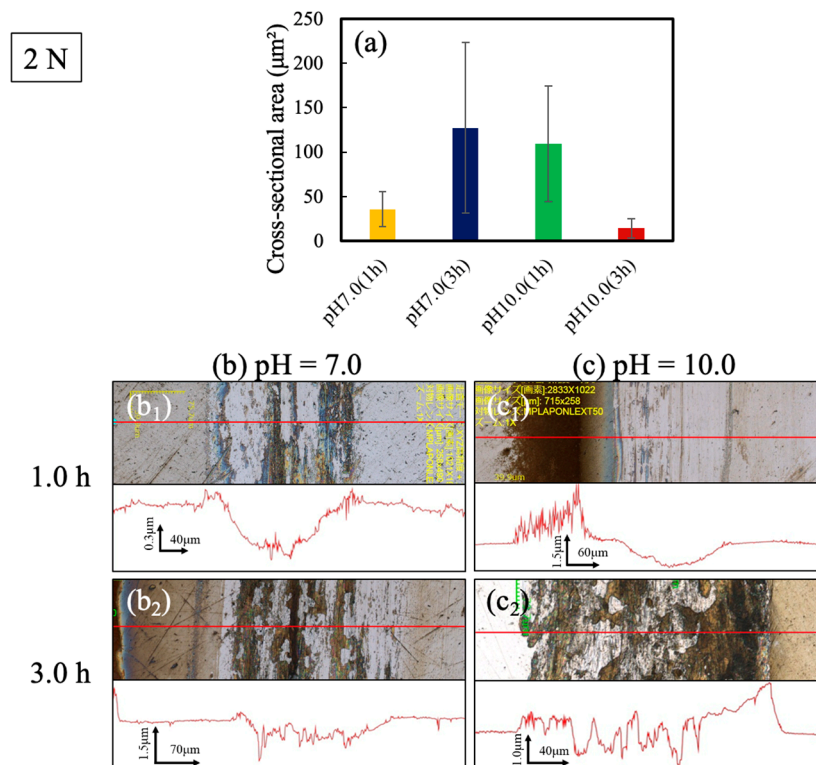


Figure 9. Grooves and the corresponding cross-sectional groove areas after tribocorrosion in solutions with pH = 7.0 (b) and 10.0 (c) under a load of 2 N for 1.0 and 3.0 h (a).

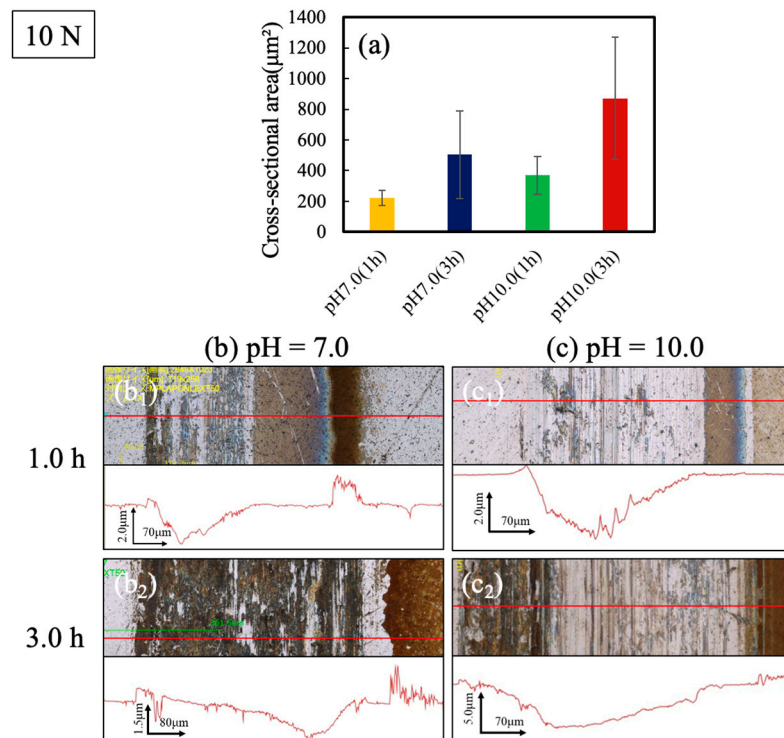


Figure 10. Grooves and the corresponding cross-sectional groove areas after tribocorrosion in solutions with pH = 7.0 (b) and 10.0 (c) under a load of 10 N for 1.0 and 3.0 h (a).

For any designated load and sliding time, the CSGAs at pH = 2.0 are larger than pH = 2.7. The larger load or the longer sliding period brought about by larger CSGA is usually described as Archard's coefficient [6]. The ratios of CSGA at pH = 2.0 for 3.0 h vs. 1.0 h are 2.8 (under 2.0 N; Figure 7) and 4.4 (under 10.0 N; Figure 8), while those at pH = 2.7 are 3.3 (under 2.0 N; Figure 7) and 3.9 (under 10.0 N; Figure 7). Under 2.0 N (Figure 7), sites of spalling from the groove surface can be seen, more in the order of pH = 2.0 after 1.0 h > 3.0 h > pH = 2.7 after 1.0 h > 3.0 h. Under 10.0 N (Figure 8), small spalling and remarkable scratches were observed.

3.3.2. Tribocorrosion in Neutral and Alkaline Solutions

As shown Figures 6c and 9, under the load of 2.0 N, the CSGA obtained at pH = 7.0 (containing 0.05 M Na_2SO_4) is near 20 times that in deionised water (absence of Na_2SO_4). The free ions in the solution should have promoted tribocorrosion through the enhanced macro-cell reaction. According to the polarization measurement (Figures 3 and 4), the corrosion in either solution with pH = 7.0 and 10.0 is slow and the passivation tendency is high. The tribocorrosion in these cases should be closely related to the cyclically destroyed and fixed passive films, which play both roles of accumulation and lubrication.

However, the tribocorrosion behaviour at pH = 7.0 and 10.0 seemed much different. Under the load of 2.0 N (Figure 9), the CSGA ratio of 3.0 h vs. 1.0 h at pH = 7.0 is 3.6. On the other hand, the CSGA at pH = 10.0 after 1.0 h is much larger than at pH = 7.0, dramatically decreasing to a much smaller value after 3.0 h. The latter is ascribed to the accumulation of wear particles, which can be inferred from the observed higher zones (right dark brown) than their surrounds. Although almost the same polarization curves were obtained at pH = 7.0 and 10.0, the passive film at pH = 10.0 was thicker [7]. The cyclic detachment of passive film at pH = 10.0 during the initial 1.0 h resulted in a large CSGA. Under the load of 10.0 N (Figure 10), the scratch from the ZrO_2 ball effectively removed the wear particle from the groove, causing a highly increased CSGA value after 3.0 h.

3.4. Comparison of Wear and Tribocorrosion Volumes

The CSGAs and groove profiles are depicted in Figures 6–10. Here, the wear and tribocorrosion volumes were further calculated from CSGA by Equation (2), as shown in Figure 11. Since all the sliding radii are set to 5.0 mm, the wear or tribocorrosion volumes are linearly proportional to CSGA. The smallest volume was obtained under either load or sliding time in the deionised water, followed by the second-smallest values at pH = 7.0 or 10.0. In these neutral and alkaline solutions, the easily formed or reformed passive film should have played an essential role in suppressing the tribocorrosion. Furthermore, fewer free ions in the deionised water enhanced the above effect.

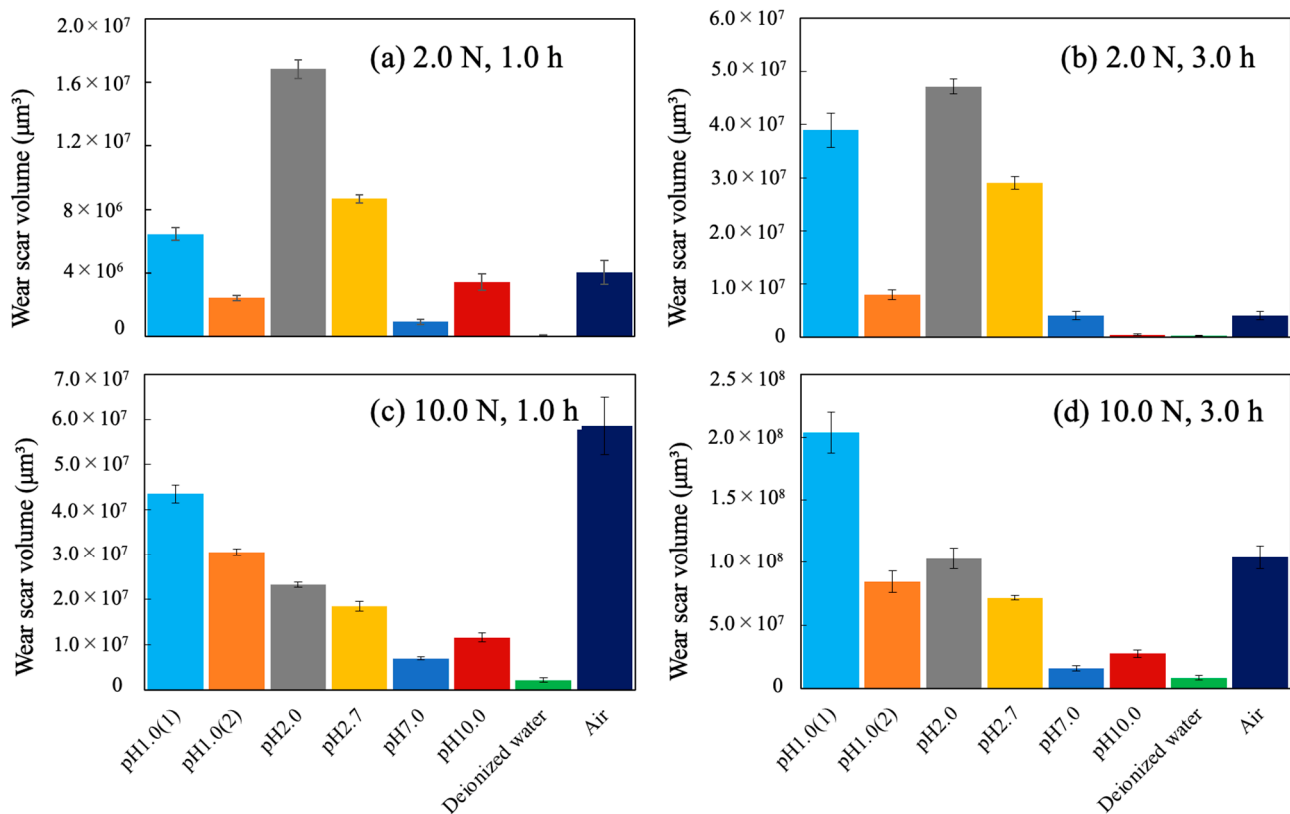


Figure 11. Groove volumes obtained under various conditions. (a) 2 N, 1.0 h, (b) 2 N, 3.0 h, (c) 10 N, 1.0 h, and (d) 10 N, 3.0 h.

Under the load of 2.0 N and after the 1.0 h sliding (Figure 11a), although the apparent corrosion only occurred at pH = 1.0, the largest tribocorrosion volume was obtained at pH = 2.0, followed by the next-largest one at pH = 2.7. The volume based on the corroded surface at pH = 1.0 was even less than that at pH = 10.0, indicating their large difference in tribocorrosion mechanisms. Under the load of 2.0 N and after the 3.0 h sliding (Figure 11b), the largest volume was also still obtained at pH = 2.0, but the second-largest one reached that at pH = 1.0. Their volumes are much larger than in the air, indicating a strong impact of corrosion. Accumulation of wear particles occurred in the air, but not in acid solutions. Under the load of 10.0 N and after the 1.0 h sliding (Figure 11c), the largest volume was obtained in the air. The second-largest volume was obtained at pH = 1.0 and gradually decreased with pH increase. The volume from the corroded surface at pH = 1.0 was larger than pH = 2.0, showing the large impact of protons on tribocorrosion. The large load enwidens the interior plastic region to the surficial side, accelerating the tribocorrosion. Under the load of 10.0 N and after the 3.0 h sliding (Figure 11d), the largest volume was obtained at pH = 1.0, while the second-largest in air depicts almost the same level as in other acid solutions. The volumes in air and solutions at pH = 2.0 and 2.7 were near that at pH = 1.0 from the corroded surface.

3.5. Comparing Coefficients of Friction and Archard Wear Coefficients

The coefficient of friction and the tribocorrosion behaviour mutually influence each other. A higher friction coefficient brings about higher shear stress to the steel. Figure 12 shows the averaged friction coefficient under the load of 2.0 N at the rotation of 60 rpm for 900 s. The error bar means the maximum and the minimum values. Note that the friction coefficient in either solution increased with the sliding time, indicating the continuously varying contact state. The friction coefficient gradually increased with the increase in pH values, while the value in deionised water was near that at pH = 10.0. Compared to air, deionised water should have played a role in lubrication through the passivated surface. In the neutral and alkaline solutions, the passive hard film with a different composition from the substrate changes the contact state. In the acid solutions without passive film, the dissolution of the metal adhered to the ball should have been promoted, resulting in a low friction force. Although the fatigue failure of the surficial and sub-surficial metal has been observed with shakedown [26], a clear relationship between friction coefficient and wear volume was not observed here, showing the complicated mechanism of the tribocorrosion.

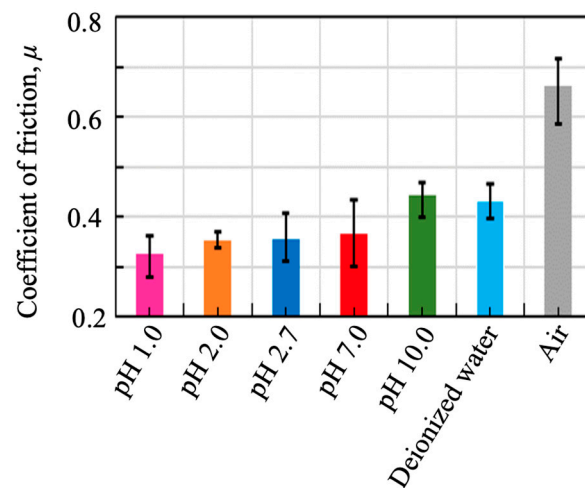


Figure 12. Coefficient of friction measured in various solutions with different pH.

The Archard wear coefficient (k) was computed by Equation (6) to express the tribocorrosion tendency under unit load and sliding period (Figure 13). Here, H is the Vickers hardness of the steel (1.7 GPa: 1.0 kg, 12.5 s, six measurements), and d is the sliding distance. The environmental factor of the pH value is not included in the equation; therefore, each k value means a property of the steel in a specific solution.

$$k = \frac{V \cdot H}{F \cdot d} \quad (6)$$

The k value largely decreased from the acid to the neutral/alkaline solution, similarly to the nonlinear relationship obtained from the steel coupled with graphite (with passive film) [6]. In acid solutions and under the load of 2.0 N, the largest k value at pH = 2.0 can be attributed to a synergistic effect from the weak scratch, the weak active corrosion, and the galvanic accelerated corrosion. Under the load of 10.0 N, the k value monotonously decreased from pH = 1.0 to 2.7, indicating that reduced corrosion played a significant role. On the other hand, except under 2.0 N for 3.0 h, the k value at pH = 10.0 was larger than pH = 7.0, which might be due to the cyclically lost thicker film at pH = 10.0. Even in a solution with the same pH, the k value varied with different loads and sliding periods. Except for the load and the sliding time, the accumulation of corrosion powder and its lubrication cannot be neglected in discussing the mechanism of tribocorrosion.

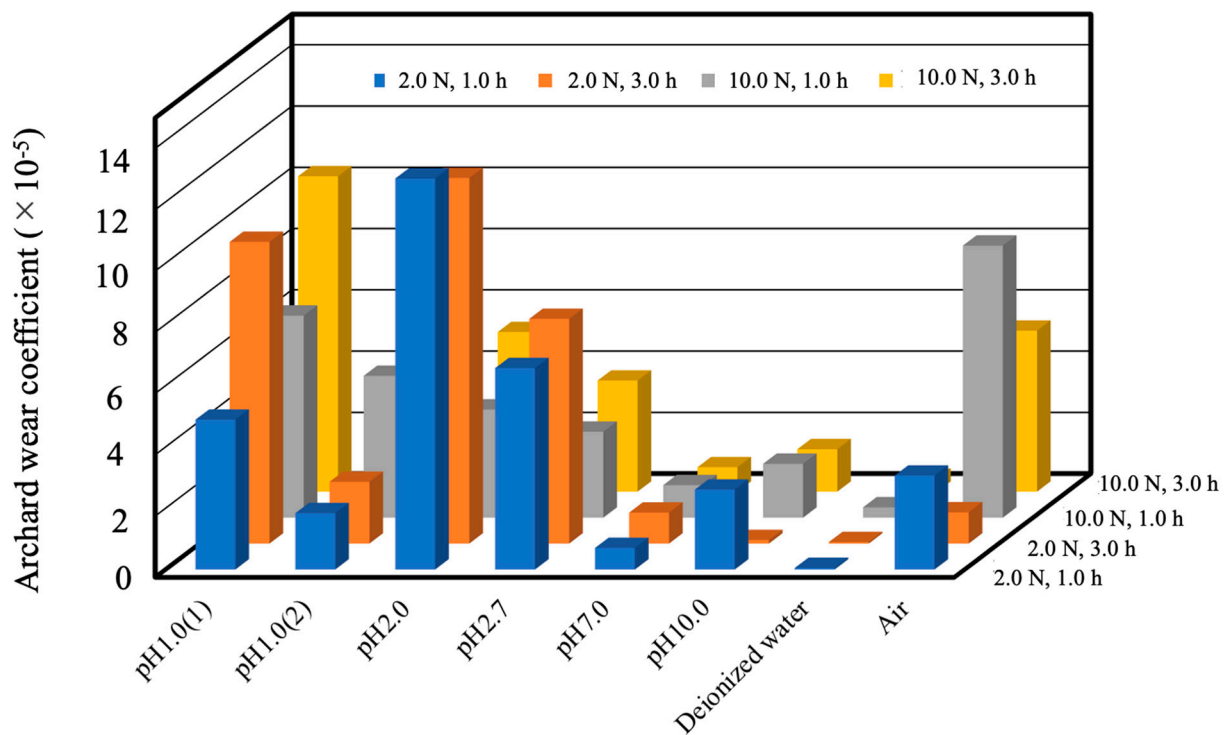


Figure 13. Archard wear coefficient under various conditions.

3.6. Synergistic Influence for Corrosion and Wear

As described before, the locally occurring tribocorrosion caused the loss of steel both from the sliding circle and from the unworn surface, either of which can be directly measured by the profile analysis. The loss of steel from the unworn surface is apparent at pH = 1.0. Furthermore, the volume of the groove includes both the corroded and the worn steel. The former electrochemically dissolved and the latter mechanically detached from the steel. They synergistically affect each other. As mentioned later, the corrosion rate at the sliding circle is not equal to either the freely immersed one or that at the unworn surface. Even measuring the concentration of the dissolved metal ions in the solution cannot be used to induce the electrochemically corroded amount, considering the self-dissolution of the loose particles from the steel. The mechanical wear is more complex than that in air or deionised water. Several papers have mentioned the combined influence of corrosion and wear in the tribocorrosion process [2,14,33–36]. Here, simply not considering the self-dissolution of the leaved particles from the steel, the total lost steel (V_t) under the ZrO_2 ball from the sliding circle in tribocorrosion can be ideally depicted as Equation (7).

$$V_t = V_{wc} + V_{cw} \quad (7)$$

V_{wc} and V_{cw} represent the mechanical wear containing that accelerated by corrosion and the chemical corrosion containing that accelerated by wear, respectively. Corrosion generally roughens and destabilizes the surface [37–39], promotes crack propagation [40,41], and dissolves the work-hardened layer [37] or the wear particle. On the other hand, wear also roughens the surface and produces the wear particle, which brings about a local electric field for corrosion [37]. Wear removes the passive film, works to harden the surface layer, and yields dislocations, which results in an unstable surface for easy corrosion [42,43]. The surface change during tribocorrosion brings about a galvanic effect on the whole surface. Therefore, the separation of V_{wc} and V_{cw} can give deep insight into the actual mechanism of tribocorrosion. Equation (7) is near that proposed by Jiang et al. [41,44], but not that proposed by Uhlig's model [14]. The latter did not consider the synergistic effect of corrosion and wear. The synergistic effect was contained in V_{wc} and

V_{cw} , but not the separately listed ones in the literature [45]. Much more compiled models containing the influence of cyclic loading, corrosion fatigue, and stress corrosion cracking were also proposed; however, experimentally distinguishing each specific effect is still challenging [44].

Only at pH = 1.0 was apparent corrosion detected on the unworn surface. Figure 14 depicts the corroded depth from the unworn surface in this case. Here, the condition of 0.0 N means free immersion, i.e., no contact of the ZrO_2 ball with the specimen. A Teflon tape protected four corners of the rectangle specimen as the uncorroded surface. After free immersion or tribocorrosion, the corrosion depth was measured between the protected and corroded surfaces. The corroded depth after 1.0 h free immersion (without sliding; 0.0 N) was also calculated from the polarization curve's current density, as shown with a white triangle in the same figure. The directly measured depth by laser microscopy and the polarization curve's calculated depth were almost identical. On the unworn surface, the corroded depth under the load of 2.0 N after 1.0 h sliding ($0.64 \mu\text{m}$) was only about half of that without load (free immersion: $1.15 \mu\text{m}$), and the depth after 3.0 h ($5.50 \mu\text{m}$) was larger than that without load (free immersion: $4.28 \mu\text{m}$). Under the load of 10.0 N, the corroded depth on the unworn surface after 1.0 h sliding was almost the same as that without load, and the depth after 3.0 h sliding ($8.34 \mu\text{m}$) was much larger than that without load ($4.28 \mu\text{m}$). Therefore, it is in no doubt that the corrosion on the unworn part was primarily affected by the sliding. Significantly, the reduced corrosion by sliding under 2.0 N for 1.0 h seems complex.

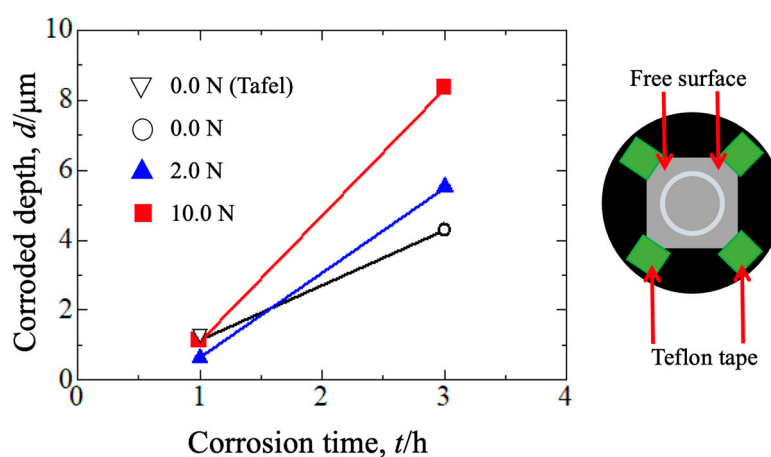


Figure 14. Corroded depths from the free or unworn surface without and with different sliding loads.

The above facts show the distribution of cathodic and anodic currents on the free surface and the unworn/sliding surface at pH = 1.0, schematically demonstrated in Figure 15 a,b. In the absence of load and sliding, equal cathodic and anodic currents are evenly distributed on either part of the surface (Figure 15a; F and F*: free surface). During the first hour of sliding, the anodic current on the unworn surface was only half that of the free immersion (Figure 14). From an additional electrochemical noise (EN) measurement, an electron flow was confirmed from the unworn part to the sliding track (W**: worn surface) (Figure 15b). Therefore, the cathodic current on the unworn surface should be weaker than its neighbouring anodic one. The anodic current on the sliding surface (corresponding V_{cw} in Equation (6)) should be weaker than its neighbouring cathodic one. Moreover, considering the hydrogen gas bubbles were removed from the sliding surface by the moving ZrO_2 ball, both the active sites for protons' reduction and the proton density on the sliding surface should be more than on the unworn surface. As a result, the cathodic current on the worn surface (Figure 15b) was reasonably higher than before applying load (Figure 15a). Tsuchiya et al. [31] also proposed a proton's increased cathodic reaction on a scratched SUS304 surface at pH = 5.6 and corrosion potential of -390 mV vs. SCE , explained by the activated surface for the reduction of protons. Accelerated corrosion on the unworn surface of carbon steel of AISI 1045 was also observed in seawater

with pH = 8.2, but the reason was not clarified [36]. On the other hand, the anodic current on the sliding surface (Figure 15b) should be lower than that without applying load (Figure 15a) because the maximum depth of the groove (1.30 μm) was very near to the corroded depth in the absence of load (1.15 μm). More work is necessary to clarify such a phenomenon. Perhaps the promoted cathodic reaction on the sliding surface occurred due to the direct removal of hydrogen bubbles and then caught electrons from the near sliding surrounds (Figure 15b: right). Next, electrons immigrated from the unworn surface (Figure 15b: left) with the cathodic reaction suppression, followed by the suppressed anodic reaction on the unworn surface. Such changed hydrogen evolution might influence the hydrogen entry behaviour in steel [46]. On the other hand, the reason for deeper corrosion under 10.0 N or for 3.0 h (Figure 14) is not known. Under the load of 2.0 N, a reversed electron flow at pH = 2.0 was confirmed in the EN measurement from the sliding track to the unworn part, which should be the reason for obtaining the severer tribocorrosion than at pH = 1.0.

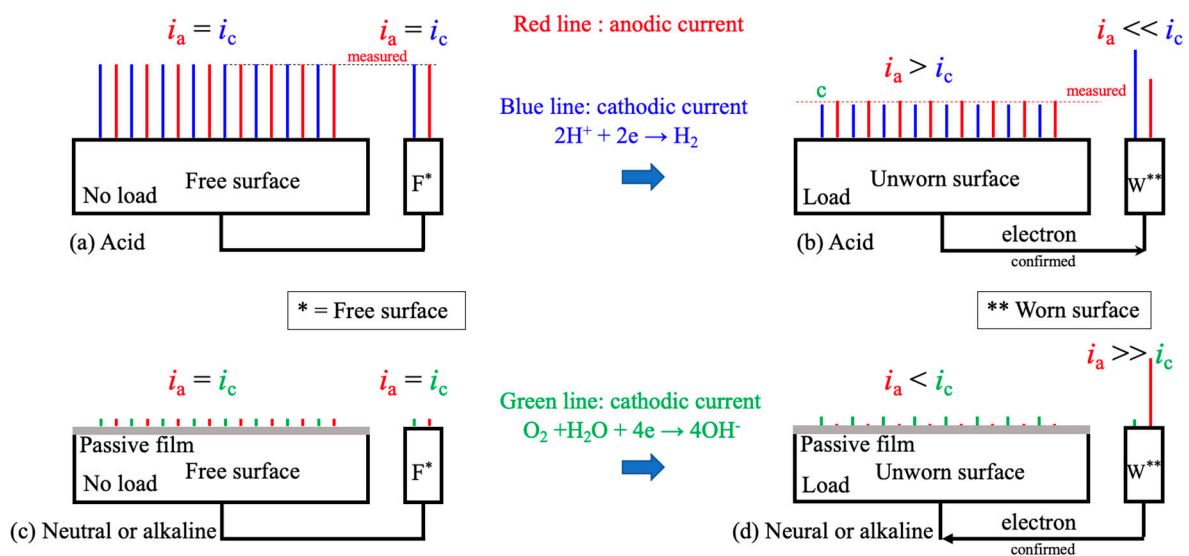


Figure 15. Anodic and cathodic distribution on the free surface (a,c), unworn surface (b,d; left), and worn surface (b,d; right) in acid solution (a,b) and neutral or alkaline solution (c,d).

Figure 15c,d show the distribution of cathodic and anodic currents on the free surface and the unworn/sliding surface in neutral and alkaline solutions. The passive film forms on the surface, resulting in an anodic current much lower than dissolved oxygen's diffusion limit current density. An electron flow from the sliding track to the unworn part with a potential drop was in situ-detected when sliding started. This phenomenon means an accelerated anodic reaction on the sliding track [37,47]. In these neutral and alkaline solutions, corrosion fatigue and stress corrosion cracking might also occur under cyclic loading, which Von Der Ohe proposed as the multi-degradation model [44].

As described before, clarifying V_{wc} and V_{cw} helps to understand the mechanism of tribocorrosion, which can promote the development of a practical assessment method. In particular, the influence of sliding on the corrosion at the unworn surface is meaningful in clarifying the whole mechanism of tribocorrosion. To clarify such tribocorrosion issues for stainless steels and other alloys, well-designed in situ measurement of electrochemical signals is necessary in future investigations.

4. Conclusions

The tribocorrosion behaviour of SUS430 stainless steel was investigated in aqueous solutions with different pH to clarify the influence of passivation. Different loads and sliding times were applied to examine the impact of plastic deformation and the accumulation of wear particles. Together with the polarization behaviour, the worn or tribocorroded surface

was observed by laser microscopy. The depth profiles of the formed groove were used to discuss the mechanism of the tribocorrosion. The obtained conclusions were as follows.

The polarization behaviour of SUS430 steel essentially changed with the pH of the solution. Passive film existed at pH = 7.0 and 10.0, but vanished at pH = 1.0 and 2.0.

The wear in the air largely depended on the applied loads. Less influence of sliding time was detected under 2.0 N due to the accumulation of wear particles. On the other hand, the tribocorrosion in deionised water was much less than the pure wear in air, partially ascribed to the low friction coefficient in water.

Depending on the load and the sliding period, spalling off from steel occurred at pH = 1.0–2.7. The formed grooves were smooth without the accumulation of wear power. Under the load of 2.0 N, the tribocorrosion at pH = 1.0 was weaker than pH = 2.0. However, the situation reversed when the load was increased to 10.0 N.

Due to slow dissolution and the cyclically reformed passive film, tribocorrosion in neutral and alkaline solutions is considerably less than in acid solutions.

Author Contributions: R.W. and M.H. designed and supervised the study. Y.O. investigated the tribocorrosion behaviour. Y.L. and T.X. measured some corrosion rates. R.W., Y.O. and M.H. discussed and wrote the paper. All authors have read and agreed to the published version of the manuscript.

Funding: This research received no external funding.

Institutional Review Board Statement: Not applicable.

Informed Consent Statement: Not applicable.

Data Availability Statement: Not applicable.

Conflicts of Interest: The authors declare no conflict of interest.

References

1. Rajahram, S.S.; Harvey, T.J.; Wood, R.J.K. Erosion-corrosion resistance of engineering materials in various test conditions. *Wear* **2009**, *267*, 244–254. [[CrossRef](#)]
2. Maher, M.; Iraola-Arregui, I.; Youcef, H.B.; Rhouta, B.; Trabadelo, V. The synergistic effect of wear-corrosion in stainless steels: A review. *Mater. Today Proc.* **2021**, *51*, 1975–1990. [[CrossRef](#)]
3. Tan, L.; Wang, Z.; Ma, Y. Tribocorrosion behavior and degradation mechanism of 316L stainless steel in typical corrosive media. *Acta Metal. Sin.* **2021**, *34*, 813–824. [[CrossRef](#)]
4. Tan, L.; Wang, Z.; Ma, Y.; Yan, Y.; Qiao, L. Tribocorrosion investigation of 316L stainless steel: The synergistic effect between chloride ion and sulfate ion. *Mater. Res. Express* **2021**, *8*, 086501. [[CrossRef](#)]
5. Zou, J.; Wang, Z.; Ma, Y.; Tan, L. Tribocorrosion behavior and degradation mechanism of 316L stainless steel in alkaline solution: Effect of tribo-film. *Acta Metal. Sin.* **2022**, *35*, 1365–1375. [[CrossRef](#)]
6. Dalbert, V.; Mary, N.; Normand, B.; Verdu, C.; Saedlou, S. In situ determinations of the wear surfaces, volumes and kinetics of repassivation: Contribution in the understanding of the tribocorrosion behaviour of a ferritic stainless steel in various pH. *Tribol. Int.* **2020**, *150*, 106374. [[CrossRef](#)]
7. Wang, R.; Li, Y.; Xiao, T.; Cong, L.; Ling, Y.; Lu, Z.; Fukushima, C.; Tsuchitori, I.; Bazzaoui, M. Using atomic force microscopy to measure thickness of passive film on stainless steel immersed in aqueous solution. *Sci. Rep.* **2019**, *9*, 13094. [[CrossRef](#)]
8. Sugimoto, K.; Matsuda, S. Passive and transpassive films on Fe-Cr alloys in acid and neutral solutions. *Mater. Sci. Eng.* **1980**, *42*, 181–189. [[CrossRef](#)]
9. Sato, N. An overview on the passivity of metals. *Corros. Sci.* **1990**, *31*, 1–9. [[CrossRef](#)]
10. Liu, C.; Wu, J. Influence of pH on the passivation behavior of 254SMO stainless steel in 3.5% NaCl solution. *Corros. Sci.* **2007**, *49*, 2198–2209. [[CrossRef](#)]
11. Wang, R. Suppression effect of ultrasound on pitting corrosion of SUS304 stainless steel in various NaCl solutions. *Sci. China Technol. Sci.* **2019**, *62*, 551–558. [[CrossRef](#)]
12. Okamoto, G. Passive film of 18-8 stainless steel structure and its function. *Corros. Sci.* **1973**, *13*, 471–489. [[CrossRef](#)]
13. Svistunova, T.V.; Shlyamnev, A.P. Development and use of corrosion-resistant steels and alloys. *Met. Sci. Heat Treat* **2010**, *52*, 300–308. [[CrossRef](#)]
14. Cao, S.; Mischler, S. Modeling tribocorrosion of passive metals—A review. *Curr. Opin. Solid State Mater. Sci.* **2018**, *22*, 127–141. [[CrossRef](#)]
15. Jemely, P.; Mischler, S.; Landolt, D. Tribocorrosion behaviour of Fe-17Cr stainless steel in acid and alkaline solutions. *Tribol. Int.* **1999**, *32*, 295–303. [[CrossRef](#)]

16. Stemp, M.; Mischler, S.; Landolt, D. The effect of mechanical and electrochemical parameters on the tribocorrosion rate of stainless steel in sulphuric acid. *Wear* **2003**, *255*, 466–475. [[CrossRef](#)]
17. Betova, I.; Bojinov, M.; Lilja, C. Influence of ionic strength on hydrogen generation during interaction of copper with deoxygenated neutral solution. *Corros. Sci.* **2021**, *188*, 109552. [[CrossRef](#)]
18. Fontana, M.G.; Staehle, R.W. *Advances in Corrosion Science and Technology: Volume 6 (Advances in Corrosion Science & Technology)*; Springer: Berlin, Germany, 1976.
19. *JIS R1613-2010*; Testing Method for Wear Resistance of Fine Ceramics by Ball-on-Disc Method. Japanese Industrial Standards Committee: Tokyo, Japan, 2010.
20. Wang, R.; Imagawa, M.; Honda, M.; Fukuhara, H.; Hiramatsu, S. Influence of dissolved oxygen on DL-EPR behavior of SUS329J4L duplex stainless steel after convection cooling. *J. Soc. Mater. Sci. Jpn.* **2020**, *70*, 49–56. [[CrossRef](#)]
21. Hara, N.; Sugimoto, K. In situ analysis of passive films by potential modulated uv-visible reflection spectroscopy. *Corros. Sci.* **1990**, *31*, 197–206. [[CrossRef](#)]
22. Nagaoka, A.; Matsushashi, R.; Nose, K.; Matsuoka, K.; Kajimura, H. The effect of chloride ion and dissolved oxygen concentration on passivation of SUS304 stainless steel. *Zair.-Kankyo/Corros. Eng. Jpn.* **2020**, *69*, 49–57.
23. Ohtsuka, T.; Fushimi, K. Optical characterization of passive oxides on metals. *Electrochemistry* **2016**, *84*, 826–832. [[CrossRef](#)]
24. Hashimoto, H. *Kiso Kara Manabu*; Morikita Publishing Co., Ltd.: Tokyo, Japan, 2006. (In Japanese)
25. Sasaki, S.; Shima, M.; Noguchi, S.; Hirayama, T.; Jibiki, T.; Adachi, K.; Miyake, K. *A 1st Course in Tribology*; Kodansha: Tokyo, Japan, 2013. (In Japanese)
26. Munoz, A.I.; Espallargas, N.; Mischler, S. *Tribocorrosion*; Springer Nature Switzerland AG: Cham, Switzerland, 2020.
27. Endou, K. *Hyoumen Kougaku*; Yokendo Ltd. Publishers: Tokyo, Japan, 1976. (In Japanese)
28. Favero, J.; Stadelmann, P.; Mischler, S. Effect of the applied potential of the near surface microstructure of a 316L steel submitted to tribocorrosion in sulfuric acid. *J. Phys. D Appl. Phys.* **2006**, *39*, 3175–3183. [[CrossRef](#)]
29. Perret, J.; Boehm-Courjault, E.; Cantoni, M.; Mischler, S.; Beaudouin, A.; Chitty, W.; Vernot, J.P. EBSD, SEM and FIB characterisation of subsurface deformation during tribocorrosion of stainless steel in sulphuric acid. *Wear* **2010**, *269*, 383–393.
30. Maldonado, S.G.; Mischler, S.; Cantoni, M.; Chitty, W.J.; Falcand, C.; Hertz, D. Mechanical and chemical mechanisms in the tribocorrosion of a Stellite type alloy. *Wear* **2013**, *308*, 213–221. [[CrossRef](#)]
31. Tsuchiya, Y.; Saito, N. Electrochemical Noise Analysis for Localized Corrosion of Type 304 Stainless Steel in Neutralized Chloride Solution. *Zairyo-to-Kanhyo* **2001**, *50*, 323–329. [[CrossRef](#)]
32. Inoue, H.; Ohnaka, N. Potential noise for stress corrosion cracking in corroding crevice—Report on the results of the cooperative experiment at the working group in Japan Society of Corrosion Engineering: “Detecting of the localized corruptions by the electro-chemical noise”. *Zairo-to-Kankyo* **2000**, *49*, 99–105. [[CrossRef](#)]
33. Burstein, G.T.; Sasaki, K. Effect of impact angle on the slurry erosion–corrosion of 304L stainless steel. *Wear* **2000**, *240*, 80–94. [[CrossRef](#)]
34. Zheng, Y.; Yao, Z.; Wei, X.; Ke, W. The synergistic effect between erosion and corrosion in acidic slurry medium. *Wear* **1995**, *186–187*, 555–561. [[CrossRef](#)]
35. Yu, Z.; Chen, M.; Li, F.; Zhu, S.; Wang, F. Synergistic effect of corrosion and wear of the 316 stainless steel in molten zinc alloy at 460 °C. *Corros. Sci.* **2020**, *165*, 108411.
36. Zhang, B.; Wang, J.; Liu, H.; Yan, Y.; Jiang, P.; Yan, F. Tribocorrosion properties of AISI 1045 and AISI 2205 steels in seawater: Synergistic interactions of wear and corrosion. *Friction* **2021**, *9*, 929–940. [[CrossRef](#)]
37. Wang, H.W.; Stack, M.M. The erosive wear of mild and stainless steels under controlled corrosion in alkaline slurries containing alumina particles. *J. Mater. Sci.* **2000**, *35*, 5263–5273.
38. Bargmann, I.; Neville, A.; Hertzman, S.; Reza, F.; Hu, X. Erosion-corrosion in oil and gas—Stainless steel under deaerated slurry impingement attack. In Proceedings of the NACE—International Corrosion Conference Series, Atlanta, GA, USA, 22–26 March 2009.
39. He, D.D.; Jiang, X.X.; Li, S.Z.; Guan, H.R. Erosion-corrosion of stainless steels in aqueous slurries—a quantitative estimation of synergistic effects. *Corrosion* **2005**, *61*, 30–36.
40. Rajahram, S.S.; Harvey, T.J.; Walker, J.C.; Wang, S.C.; Wood, R.J.K. Investigation of erosion-corrosion mechanisms of UNS S31603 using FIB and TEM. *Tribol. Int.* **2012**, *46*, 161–173.
41. Jiang, J.; Stack, M.M.; Neville, A. Modelling the tribo-corrosion interaction in aqueous sliding conditions. *Tribol. Int.* **2002**, *35*, 669–679.
42. Lindgren, M.; Siljander, S.; Suihkonen, R.; Pohjanne, P.; Vuorinen, J. Erosion–corrosion resistance of various stainless steel grades in high-temperature sulfuric acid solution. *Wear* **2016**, *364–365*, 10–21.
43. Guo, H.X.; Lu, B.T.; Luo, J.L. Interaction of mechanical and electrochemical factors in erosion-corrosion of carbon steel. *Elec-trochim. Acta* **2005**, *51*, 315–323.
44. von der Ohe, C.B.; Johnsen, R.; Espallargas, N. Modeling the multi-degradation mechanisms of combined tribocorrosion in-teracting with static and cyclic loaded surfaces of passive metals exposed to seawater. *Wear* **2010**, *269*, 607–616.

45. G119 04; Standard Guide for Determining Synergism Between Wear and Corrosion. ASTM International: West Conshohocken, PA, USA, 2004.
46. Doi, K.; Akiyama, E. Hydrogen entry into a high strength steel with tribocorrosion in acidic solution. *Trans. JSSE* **2017**, *2017*, 9–14.
47. Papageorgiou, N.; Mischler, S. Electrochemical simulation of the current and potential response in sliding tribocorrosion. *Tribol. Lett.* **2012**, *48*, 271–283.

Disclaimer/Publisher’s Note: The statements, opinions and data contained in all publications are solely those of the individual author(s) and contributor(s) and not of MDPI and/or the editor(s). MDPI and/or the editor(s) disclaim responsibility for any injury to people or property resulting from any ideas, methods, instructions or products referred to in the content.